Journal of Medicinal Chemistry

Article

pubs.acs.org/jmc

Synthesis and Biological Profile of the pan-Vascular Endothelial Growth Factor Receptor/Tyrosine Kinase with Immunoglobulin and Epidermal Growth Factor-Like Homology Domains 2 (VEGF-R/TIE-2) Inhibitor 11-(2-Methylpropyl)-12,13-dihydro-2-methyl-8-(pyrimidin-2-ylamino)-4*H*-indazolo[5,4-a]pyrrolo[3,4-c]carbazol-4-one (CEP-11981): A Novel Oncology Therapeutic Agent

Robert L. Hudkins,* Nadine C. Becknell, Allison L. Zulli, Ted L. Underiner, Thelma S. Angeles, Lisa D. Aimone, Mark S. Albom, Hong Chang, Sheila J. Miknyoczki, Kathryn Hunter, Susan Jones-Bolin, Hugh Zhao, Edward R. Bacon, John P. Mallamo, Mark A. Ator, and Bruce A. Ruggeri*

Discovery Research, Cephalon, Inc., 145 Brandywine Parkway, West Chester, Pennsylvania 19380, United States

ABSTRACT: A substantial body of evidence supports the utility of antiangiogenesis inhibitors as a strategy to block or attenuate tumor-induced angiogenesis and inhibition of primary and metastatic tumor growth in a variety of solid and hematopoietic tumors. Given the requirement of tumors for different cytokine and growth factors at distinct stages of their growth and dissemination, optimal antiangiogenic therapy necessitates inhibition of multiple, complementary, and nonredundant angiogenic targets. 11-(2-Methylpropyl)-12,13-dihydro-2-methyl-8-(pyrimidin-2-ylamino)-4*H*-indazolo[5,4-a]pyrrolo[3,4-c]carbazol-4-one (**11b**, CEP-11981) is a potent orally active inhibitor of multiple targets (TIE-2, VEGF-R1, 2, and 3, and FGF-R1) having essential and nonredundant roles in tumor angiogenesis and vascular maintenance. Outlined in this article are the design strategy, synthesis, and biochemical and pharmacological profile for **11b**, which completed Phase I clinical assessing safety and pharmacokinetics allowing for the initiation of proof of concept studies.

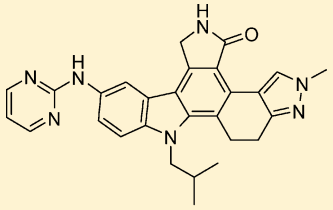

11b (CEP-11981)

INTRODUCTION

Angiogenesis, the development of new blood vessels from the endothelium of a pre-existing vasculature, is a critical process required by the majority of solid tumors to maintain localized growth and metastatic dissemination within the host.[1] The clinical application of kinase inhibitors and antivascular endothelial growth factor (VEGF) antibodies to halt angiogenesis in tumors has been validated as a therapeutic strategy by positive clinical results with bevacizumab,[2] sorafenib **1**,[3] sunitinib **2**,[4] and pazopanib **3**[5] (Figure 1). The dual vascular endothelial growth factor receptor kinase 2/fibroblast growth factor receptor 1 (VEGF-R2/FGF-R1) inhibitor **4** (brivanib, BMS-582664) advanced to phase III.[6] There is a substantial body of literature detailing the utility of antiangiogenesis inhibitors as a strategy to block or attenuate tumor-induced angiogenesis and inhibit primary and metastatic tumor growth in a variety of solid and hematopoietic tumor models. Given the heterogeneity and organ-specificity of the tumor-associated vasculature and the requirement of tumors for different cytokine and growth factors at distinct stages of their growth and dissemination, optimal antiangiogenic therapies may necessitate the inhibition of multiple, complementary, and nonredundant angiogenic targets.[7] Several angiogenic ligands and their corresponding receptor tyrosine kinases have been implicated in angiogenesis and vasculogenesis, acting at distinct phases spatially and temporally in the angiogenic process in coordinated and complementary roles to that of the VEGF–VEGF-R kinase axes. Principal among these is the angiopoietin

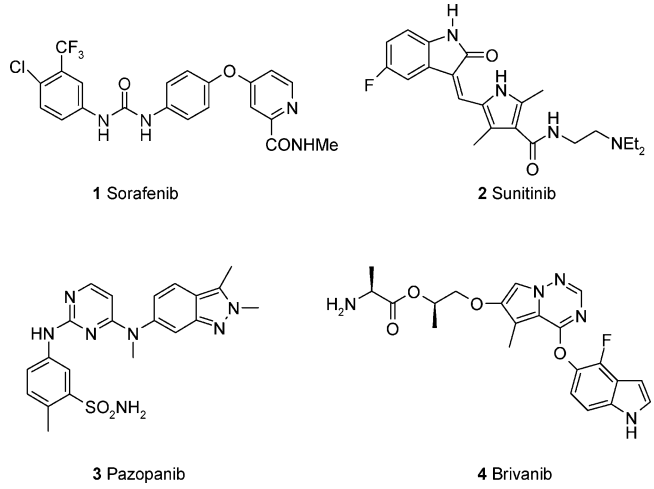

1 Sorafenib

2 Sunitinib

3 Pazopanib

4 Brivanib

Figure 1. Structures of angiogenesis inhibitors.

Received: October 26, 2011
Published: December 12, 2011

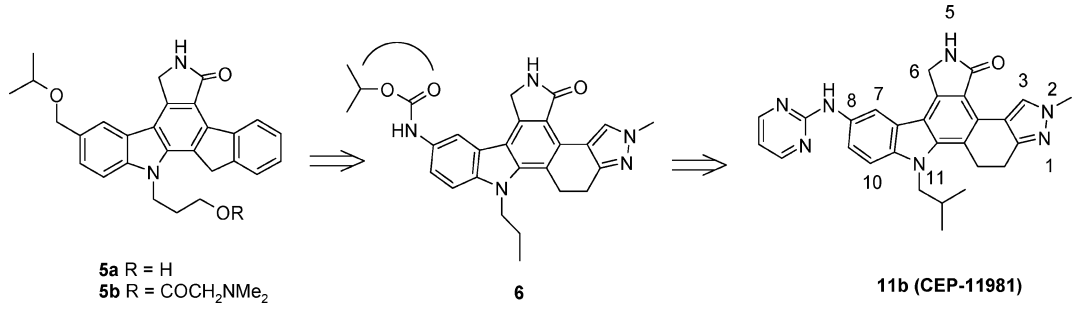

Figure 2. First and second generation angiogenesis inhibitors.

family of angiogenic growth factors (Ang-1−4) and their endothelial cell-specific receptor tyrosine kinases, tyrosine kinase with immunoglobulin and EGF-like domains 1 and 2 (TIE-1 and TIE-2), which have been implicated in vessel stabilization, maturation, and remodeling, and the proper hierarchical organization of the rudimentary vasculature.[8]

The inhibition of tumor angiogenesis and vascular remodeling achieved in nonclinical studies by modulating the angiopoietin-TIE-2 axis alone, and in concert with the VEGF−VEGF-R2 axis, has been demonstrated using biochemical, molecular, and small molecule-based approaches against a variety of human tumors.[9] Application of adenoviral delivered anti-TIE-2 and anti-VEGF-R2 have also demonstrated improved activity when both the TIE-2 and VEGF-R2 signaling pathways are targeted relative to targeting each pathway alone.[10] Inhibition of multiple angiogenic targets such as VEGF-R2 and TIE-2 are currently being evaluated clinically and preclinically.[11]

Previously, we reported on our first generation VEGF-R candidate **5b** (CEP-7055), a prodrug of **5a** (CEP-5214).[12] Indenocarbazole **5a** had potent activity for VEGF-R1, R2, and R3 (Figure 2) but had weak activity for TIE-2 (IC_{50} > 10 μM) as well as several other angiogenesis targets.[12a] The objective for a second generation follow-on compound was to design in TIE-2 activity and advance a broad-based angiogenesis inhibitor with superior biochemical, pharmacokinetic (PK), pharmacodynamic and in vivo antitumor efficacy compared to that of **5b**. As outlined in a series of publications, structural modification to the indenocarbazole core identified the N2-methyl-12,13-dihydroindazolo[5,4-*a*]pyrrolo[3,4-c]carbazole scaffold (DHI) with improved dual activity and PK properties for further lead optimization.[13] Modification to the 8-position identified several series and leads with cellular potency, PK, and in vivo antitumor efficacy such as tetrahydropyrans (THP),[13d] oximes,[13c] thienyl ketones,[13b] and carbamates.[13a] The isopropyl carbamate **6** met the dual TIE-2/VEGF-R2 enzyme (VEGF-R2 IC_{50} = 5 nM; TIE-2 = 11 nM) and cellular potency criteria (VEGF-R2 cell IC_{50} < 10 nM) and showed significant dose-related antitumor efficacy at oral doses as low as 0.3 mg/kg bid.[13a] However, **6** suffered from suboptimal pharmacokinetic properties and showed dose-limited toxicity that prevented further advancement. An additional concern for **6** and the carbamate/urea series was the theoretical toxicity associated with the potential aniline metabolite. Therefore, motivated to remove the aniline red flag and improve the pharmacokinetic properties, a series of constrained pyrimidinyl-2-amines were designed as bioisosteric replacements for the carbamate/urea moiety. In this article, we report the synthesis and structure−activity relationships (SAR) for the 2-pyrimidin-2-ylamine-DHI series and the identification of the clinical candidate **11b**.

CHEMISTRY

The 8-(pyrimidin-2-ylamino)-4*H*-indazolo[5,4-*a*]pyrrolo[3,4-c]carbazol-4-one analogues were synthesized from 5-cyano-4-ethoxycarbonyl-12,13-dihydro-2-methyl-indazolo[5,4-*a*]-carbazole intermediate **7**.[13] The DHI core and intermediate **7** were constructed via a regioselective Diels−Alder reaction as described in detail previously.[14] The key transformation to elaborate the N^{11} position for SAR development was the efficient N-alkylation of **7** to cyano-esters **8a−c** using NaOH in acetone, without hydrolysis of the ester or nitrile. Alkylation at the lactam stage produced multiple inseparable mixtures including the mono and N,N-dialkylated products. Intermediates **8a−c** were selectively nitrated at the C-8 position to give **9a−c** using exactly two equivalents of HNO_3 in AcOH at 80 °C for 1 h.[14a] A one-pot, reductive cyclization procedure was developed to convert the nitro-cyano-esters **9a−c** (Raney-Ni/H_2 in DMF-MeOH) to the amino-lactam intermediates **10a−c**.[14d] Anilines **10a−c** were reacted with 2-chloropyrimidines, 4-chloro-pyridine, or 2-chloropyridazine at *n*-butanol or *t*-butanol reflux to efficiently produce the target amino-heteroaryls **11a−j** (Scheme 1). The

Scheme 1.[a]

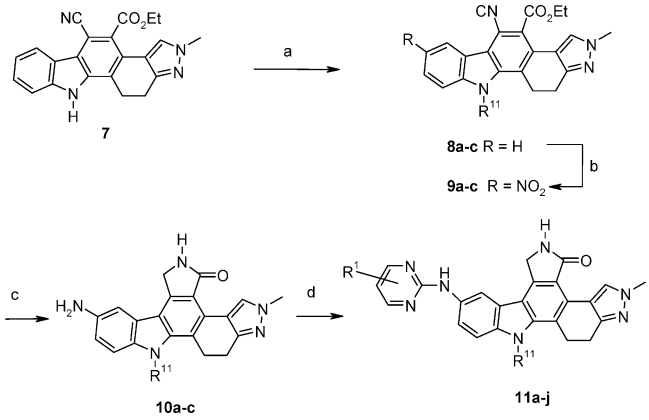

[a]Reagents and conditions: (a) alkyl iodide, NaOH, acetone, reflux, 18 h, 87−93% ; (b) HNO_3, AcOH, 80 °C, 1 h 70−87%; (c) H_2, Raney-Ni, DMF-MeOH, 81−97%; (d) heteroaryl-chloride, 1-butanol, reflux, 40−65%.

1-methyl regioisomer **15** was synthesized for comparison in an analogous manner starting with 5-(1*H*-indol-2-yl)-1-methyl-6,7-dihydro-1*H*-indazole **12** (Scheme 2).[13c,d,14a−c]

RESULTS AND DISCUSSION

In Vitro VEGF-R2 and TIE-2 Structure−Activity Relationships. The pyrimidin-2-ylamino DHI analogues were

dx.doi.org/10.1021/jm201449n | J. Med. Chem. 2012, 55, 903−913

Scheme 2.[a]

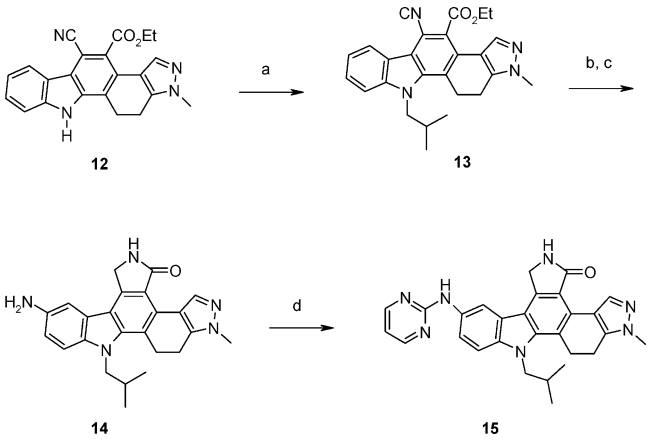

[a]Reagents and conditions: (a) 1-iodo-2-methyl-propane, NaOH, acetone, reflux, 18 h, 90%; (b) HNO_3, AcOH, 80 °C, 1 h, 85%; (c) H_2, Raney-Ni, DMF-MeOH, 80% ; (d) 2-chloropyrimidine, 1-butanol, reflux, 45%.

screened against recombinant human VEGF-R2 and TIE-2 using a heterogeneous time-resolved fluorescence (TRF) readout and recombinant human phospholipase C-γ/glutathione *S*-transferase (GST) as substrate.[12a,13] The enzyme inhibitory data is shown in Table 1. Dual TIE-2/VEGF-R2 inhibitors with IC_{50} values less than 25 nM that demonstrated acceptable cell potency, and pharmacokinetic properties were advanced for in vivo evaluation. Previous dual TIE-2/VEGF-R2 SAR studies on the core revealed that a three or four carbon alkyl unit at *N*-R^{11} was optimum for balanced dual potency and PK.[13a−c] Ideal dual target potency and PK properties were achieved with an *n*-propyl, *i*-propyl, and *i*-butyl group and further increasing or decreasing the size of the R^{11} alkyl reduced the balanced dual profile. In the pyrimidinyl-amine series, the focus was therefore on optimizing 8-pyrimidinyl-amine region while maintaining the best R^{11} alkyl. The constrained pyrimidinyl *n*-propyl **11a** retained dual potency with VEGF-R2 and TIE-2 IC_{50} values of 6 nM and 27 nM, respectively. Varying the *N*-R^{11} alkyl to *i*-butyl **11b** showed comparable potency (VEGF-R2 IC_{50} = 4 nM; TIE-2 IC_{50} = 22 nM), while *i*-propyl **11c** had a 3-fold drop in TIE-2 potency (VEGF-R2 IC_{50} = 3 nM; TIE-2 IC_{50} = 76 nM) and did not meet discovery criteria. Metabolic stability studies were conducted on **11a** and **11b** using hepatic S9 fractions from mouse, rat, dog, monkey, and human. Both compounds showed 65−77% of the parent remaining after 2 h in mouse, rat, and dog liver S9, while monkey was lower (**11a** = 44%; **11b** = 54%). In human S9, **11b** showed 79% remaining after 2 h compared to **11a**, which was 54%. Compounds **11a** and **11b** were further evaluated for pharmacokinetic properties in the rat. Compound **11b** showed acceptable oral exposure and intrinsic pharmacokinetic parameters in the rat (Table 2), while the oral exposure for **11a** (% F = 22) was lower. The oral bioavailability for **11b** was 44% after determining the plasma level exposure after i.v. (0.8 mg/kg) and p.o. (5 mg/kg) administration over a 24 h period. The i.v. terminal half-life was 1.9 h (oral half-life = 3 h), with a volume of distribution of 1.3 L/kg and a low clearance rate of 4.3 mL/min/kg. Compound **11b** also showed acceptable selectivity against CYP isoforms 2D6, 3A4, and 2C19 (IC_{50} > 30 μM for 3A4 and 2D6; 9 μM for 2C19) and no issues with CYP3A4 induction. The permeability was evaluated in the Caco-2 intestinal epithelial cell line where it was classified as high permeability (Papp = > 4 × 10^{-6} cm/sec). Compound **11b** binding to human plasma proteins was 95%, markedly lower than that of approved kinase inhibitors such as dasatinib, sorafenib, lapatanib, or nilotinib.[15] Next, the effect of substitution around the pyrimidine ring was explored with selected alkyl, methoxy, and CF_3 groups. The 5-ethylpyrimidinyl showed improved TIE-2 potency about 6-fold with an *n*-propyl (**11d**: TIE-2 IC_{50} = 4 nM) and 2-fold with an isobutyl (**11e**: TIE-2 IC_{50} = 10 nM). However, both **11d** and **11e** showed poor metabolic stability and poor rat pharmacokinetic properties and were not further advanced. The SAR further revealed that substitutions in the 4-position or combined 4,6-positions were not tolerated. 4-Methoxy **11g** and 4-trifluoromethyl **11h** reduced VEGF-R2 and abolished TIE-2 activity, while 4,6-dimethyl **11f** abolished both VEGF-R2 and TIE-2 activity. The requirement for the pyrimidinyl group for TIE-2 activity was further demonstrated by changing it to a 3-pyridazinyl **11i** or 4-pyridyl **11j**, both of which were weak to inactive for TIE-2. The position of the methyl group was important as the 1-methyl isomer **15** displayed IC_{50} values that were 11- and 16-fold weaker compared with the corresponding N-2 methyl **11b**.

The VEGF-R2 cellular activity was evaluated using a porcine endothelial cell line transfected with a chimeric receptor consisting of the extracellular portion of rat TRK-A (rTRK-A) and the intracellular domain of human vascular endothelial growth factor receptor (VEGF-R2/KDR) as described previously.[13] In general, the series demonstrated very potent cellular activity. Ligand induced stimulation of VEGF-R2 phosphorylation was blocked by **11a−e** with IC_{50} values of less than 10 nM. Further, **11b** inhibited ligand-induced human TIE-2 phosphorylation in an analogous rTRK-A-human TIE-2 chimeric endothelial cell line with an IC_{50} value of approximately 50 nM, in acceptable agreement with the enzyme activity on isolated recombinant human TIE-2 (IC_{50} = 22 nM). On the basis of the enzyme and cellular dual target potency and metabolic and pharmacokinetic profiles, **11b** was selected for advanced discovery flow profiling,

Selectivity Profile for 11b. Compound **11b** was screened for kinase selectivity against a panel of 126 kinases at 1 μM screening concentration and 100 μM ATP concentration (Upstate KinaseProfiler). The $S(90)_{126}$ value was 0.18 (fraction of kinases inhibited greater than 90%). In a separate screen of 101 selected kinases using an ATP concentration close to the K_m of the enzyme showed a comparable and favorable selectivity $S(90)_{101}$ value of 0.15. Subsequent IC_{50} values were generated for 23 kinases that demonstrated greater than 80% inhibition. In addition to TIE-2 (22 ± 6 nM) and VEGF-R2 (4 ± 1 nM), compound **11b** demonstrated inhibitory activity against angiogenesis targets VEGF-R1 (3 ± 1 nM) and FGF-R1 (13 ± 2) with IC_{50} values within the potency range observed for inhibition of the primary targets. Compound **11b** also inhibited TRK-A (IC_{50} = 3 nM), TRK-B (IC_{50} = 5 nM), Ret (IC_{50} = 5 nM), BLK (IC_{50} = 8 nM), TAK1 (IC_{50} = 14 nM), and MST2 (21 nM) with IC_{50} values less than 25 nM (Table 3). Compound **11b** showed weak activity for ABL, ALK, CDKs, CHK2, cMET, EGFR, GSK3β, IGF-R1, IRK, JAK2, JNKs, MEK, MKKs, PDGFR, PKBs, and PKCs. A broad profile screen of **11b** in binding assays for 75 receptors, ion channels, and transporters (Cerep screen) revealed 7 targets (adenosine A_{2A}, A_3; angiotensin AT1; muscarinic M_2 and M_4; neurokinin NK_1 and NK_2) that displayed ≥80% inhibition at a screening concentration of 10 μM. Follow-up K_i values revealed generally weak activity for these targets, with the adenosine A_{2A} receptor displaying the most potent activity with a K_i

dx.doi.org/10.1021/jm201449n | J. Med. Chem. 2012, 55, 903−913

Table 1. In Vitro TIE-2 and VEGF-R2 Data

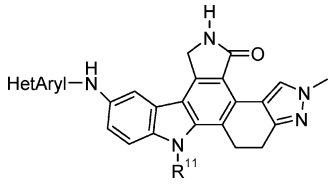

Entry	Heteroaryl	R^{11}	VEGF-R2[a]	TIE-2[a]	VEGF-R2 Cells[a,b]
11a		nPr	6 ± 2	27 ± 9	<10
11b		iBu	4 ± 1	22 ± 6	< 10
11c		iPr	3 ± 1	76 ± 5	< 10
11d	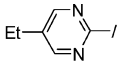	nPr	9 ± 1	4 ± 1	< 10
11e	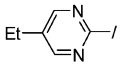	iBu	14 ± 2	10 ± 5	< 10
11f	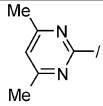	iBu	>3000	>3000	NT
11g	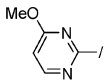	iBu	32 ± 14	>1000	NT
11h	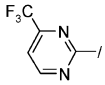	iBu	271 ± 93	>3000	NT
11i		iPr	10 ± 4	166 ± 36	NT
11j		iPr	256 ± 43	>3000	NT
15[c]		iBu	63 ± 10	241 ± 65	NT

[a]IC_{50} in nM ± SEM. [b]NT = not tested. [c]N1 methyl analogue.

Table 2. Pharmacokinetic Properties of 11b

		rat[a]	monkey[b]
i.v.	$t_{1/2}$ (h)	1.9	1.7
	V_d (L/kg)	1.3	2.6
	CL (mL/min/kg)	4.3	18
p.o.	AUC (ng·h/mL)	8559	2482
	C_{max} (ng/mL)	1330	491
	$t_{1/2}$ (h)	3.0	2.4
	t_{max} (h)	2	2
	F (%)	44	93

[a]Male rat administered at 0.8 mg/kg i.v. and 5 mg/kg p.o. Parameters were calculated from composite mean plasma concentration−time data (n = 12). [b]Administered at 0.5 mg/kg i.v. and 3 mg/kg p.o. for monkey. Parameters were calculated using plasma concentration−time data for individual animals (monkey n = 4).

value of 0.5 μM and the muscarinic M_4 subtype the weakest activity with a K_i of 2.9 μM. In addition, **11b** showed acceptable selectivity for the hERG channel with an IC_{50} value of 20 μM in Chinese Hamster Ovary cells and did not produce any significant effects on QTc interval or on action potential duration in vitro in the dog Purkinje fiber assay.

Molecular Modeling. A TIE-2 cocrystal structure with a THP-DHI analogue (PDB code 3L8P) was solved at 2.4 Å resolution was subsequently used for docking experiments with new analogues.[13d,16a] Compound **11b** docked in the TIE-2 model represents a DFG-in Type I kinase inhibitor binding mode.[16b,c] Key interactions identified in the predicted model were the lactam NH/CO bidentate donor/acceptor with Glu903 (gk +1)/Ala905 (gk +3) at the hinge region, the N1 pyrimidine nitrogen H-bonding with Asp982 (DFG) backbone amide, and the amino potential NH donor with the Asp982 side chain (Figure 3). The 8-pyrimidine moiety occupies a hydrophobic pocket flanked by gatekeeper Ile902 and Phe983 (DFG-in), with the cavity defined by Leu903, Leu888, Ile886, Leu876, and Leu985.

dx.doi.org/10.1021/jm201449n | J. Med. Chem. 2012, 55, 903−913

Table 3. Kinase Selectivity Data for 11b

kinase	IC_{50} (nM)
ALK (h)	132
AURK-A (h)	42
BLK (m)	8
BTK (h)	93
CHK2 (h)	140
CK1	48
cSRC (h)	37
FGF-R1 (h)	13
FGF-R3 (h)	89
VEGF-R1 (h)	3
FLT3 (h)	71
FMS (h)	78
MST2 (h)	21
PDGF-Rα (h)	246
RET (h)	5
TAK1(h)	14
TRK-A (h)	3
TRK-B (h)	5

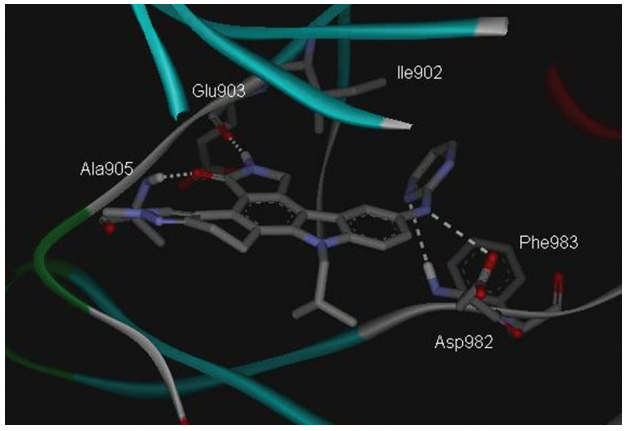

Figure 3. Predicted binding mode of **11b** with TIE-2.

A similar exercise was carried out to explore putative binding interactions of **11b** with a DFG-in inhibitor binding model of VEGF-R2 described previously.[12a,13b−d] The proposed binding mode for **11b** was consistent with the lactam moiety mimicking the ATP donor−acceptor interactions at the hinge region with the lactam N−H sharing a hydrogen bond with the Glu917 carbonyl and the lactam C═O accepting a hydrogen bond with the backbone amide of Cys919. The pyrimidine occupied the hydrophobic pocket analogous, as reported, with **5a** with the N1 nitrogen forming a significant hydrogen bond with Asp1046 and the N3 nitrogen potentially interacting with a Lys868 (not shown).[12a,13d]

Pharmacokinetic Properties of 11b in Rats and Monkeys. Compound **11b** was absorbed with higher oral bioavailability in monkeys (F = 93%) and slightly lower in rats (F = 44%). In rats, the systemic clearance was low relative to the estimated hepatic plasma flow, and the volume of distribution was approximately equal to total body water. In monkeys, the i.v. half-life ($t_{1/2}$ = 1.7 h) was comparable to that in rat, but the clearance (18 mL/min/kg) and the volume of distribution (2.6 L/kg) were larger (Table 2). The oral T_{max} was 2 h in both species, consistent with the oral half-life. An oral dose escalation study in rat (10, 30, 55, and 100 mg/kg po) showed dose-dependence near proportional exposure up to 55 mg/kg, with further dose related exposure to 100 mg/kg p.o. In monkeys (5, 25, and 100 mg/kg p.o.), a similar experiment showed dose dependent exposure to 100 mg/kg.

In Vitro and Ex Vivo Antiangiogenic Profile of 11b. The antiangiogenic activity of **11b** was evaluated in both functional (ex vivo rat aortic ring explant cultures) and target-directed (in vitro HUVEC capillary-tube formation) bioassays in order to assess their antiangiogenic activities and potential cytotoxic profiles in primary cell and organ cultures upon prolonged exposure.[17] Figure 4A,B summarizes the results obtained with **11b** in the ex vivo rat aortic ring collagen gel explants in serum-free conditions and in vitro HUVEC capillary tube formation assays. Compound **11b** exhibited dose-related inhibitory effects on peak phase microvessel growth (day 8−10 in culture) in rat aortic ring explants in 3D-collagen gels under serum-free conditions with an EC_{50} of approximately 4 nM, and inhibition of complete capillary-tube formation by HUVECs on Matrigel with an EC_{50} of approximately 2 nM. These effects were observed in the absence of apparent cytotoxicity. In addition to the potential synergistic effects of TIE-2 and pan-VEGF-R inhibition on the readout of these bioassays, the contributions of additional kinase inhibitory properties by **11b** (for e.g. FGF-R1) may contribute to the significant antiangiogenic activities observed. To evaluate inhibition of TIE-2-mediated biological activity independent of VEGF-R, the dose-related inhibition of recombinant human angiopoietin 1-stimulated HUVEC chemotaxis was evaluated in a modified Boyden chamber assay. Compound **11b** exhibited significant inhibitory activity against Ang-1-stimulated HUVEC chemotaxis at concentrations ≥50 nM in absence of HUVEC cytotoxicity (data not shown). This result is consistent with the human TIE-2 IC_{50} for **11b** (Table 1). Similarly, in vitro bioassays evaluating VEGF- and FGF-induced effects on the proliferation, migration, and survival of HUVEC, HMVEC, and BAEC demonstrated EC_{50} values of 8−38 nM (data not shown), consistent with the biological activities highlighted above. Collectively, these data confirm the robust, dose-related antiangiogenic activity of **11b** across a panel of target-directed bioassays.

In Vivo Profile for 11b. The in vivo antitumor efficacy of **11b** was assessed on the A375 human melanoma and U251MG human glioblastomas, two highly angiogenic VEGF-R2 and TIE-2 dependent solid tumors. Oral administration of **11b** (1.0 to 30 mg/kg bid; Tween: methylcellulose) to nude mice bearing established U251MG human glioblastoma xenografts resulted in a sustained dose-related (3 mg/kg, 61% ($p < 0.01$); 10 mg/kg, 75% ($p < 0.001$); and 30 mg/kg, 88% ($p < 0.001$)) maximum inhibition of tumor xenograft growth relative to that of vehicle-treated controls after 29 days with a minimum effective dose (MED) of 3 mg/kg bid (Figure 5 and Table 4). A 20% and 44% incidence of partial tumor regressions was achieved with 10 and 30 mg/kg bid, respectively. At 30 mg/kg bid C_{max} plasma and tumor levels of **11b** were 1200 ± 79 ng/mL and 401 ± 62 ng/g, respectively. Similarly, oral administration of **11b** to nude mice bearing established A375 human melanoma xenografts resulted in a MED of 0.3−1 mg/kg bid for sustained antitumor efficacy. Significant inhibition of A375 tumor xenograft growth (maximally 98% at 10 mg/kg bid; $p < 0.001$) and sustained partial and complete tumor regressions (maximally 50% and 40%, respectively, at 10 mg/kg bid) were achieved and were directly related to tumor and plasma exposure (Figure 6 and Table 4). At 10 mg/kg bid, C_{max}

dx.doi.org/10.1021/jm201449n | J. Med. Chem. 2012, 55, 903−913

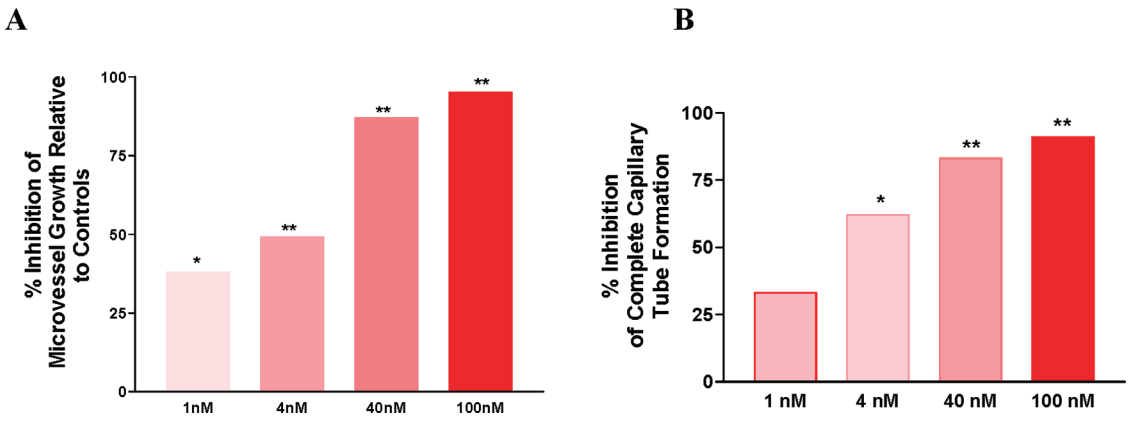

Figure 4. Antiangiogenic activity of **11b** ex vivo rat aortic ring explant cultures and in vitro HUVEC capillary-tube formation bioassays. Ex vivo rat aortic ring explant cultures and target-directed in vitro HUVEC capillary-tube formation to assess their antiangiogenic activities and potential cytotoxic profiles in primary cell and organ cultures. Compound **11b** exhibited dose-related inhibitory effects on peak phase microvessel growth (day 8−10 in culture) in rat aortic ring explants in 3D-collagen gels under serum-free conditions with an EC_{50} of approximately 4 nM, and inhibition of complete capillary-tube formation by HUVECs on Matrigel with an EC_{50} of approximately 2 nM. $P < 0.05$**, $p < 0.01$* relative to control cultures.

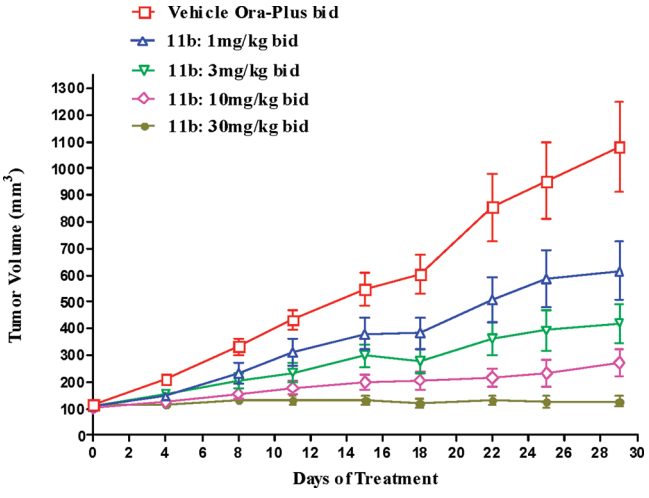

Figure 5. Oral antitumor activity of **11b** in the U251 MG human glioblastoma xenograft. Tumor cells were injected subcutaneously in serum-free media into the right flank of athymic female nude mice. Twelve days post-implantation, mice with established tumors were randomized into treatment groups (n = 10 mice/group) and administered **11b** orally (100 μL/dose) at the doses indicated and tumor volumes measured as defined in the Experimental Section. Statistical analyses for efficacy of **11b** are detailed in Table 4.

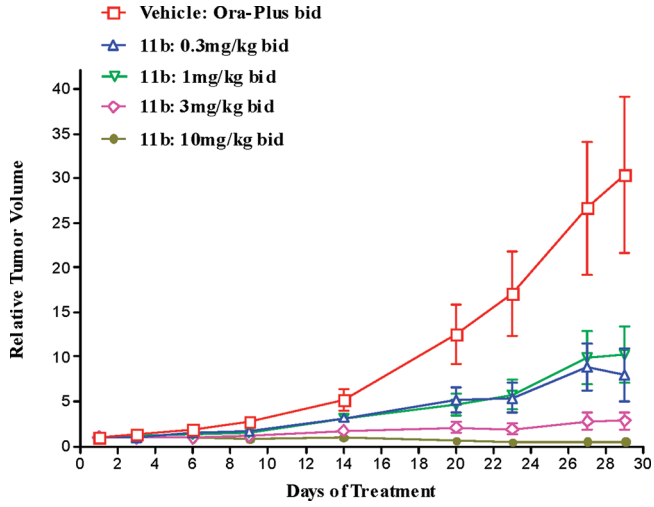

Figure 6. Oral antitumor activity of **11b** in the A375 human melanoma xenograft model. Tumor cells were injected subcutaneously in serum-free media into the right flank of athymic female nude mice. Ten days post-implantation, mice with established tumors were randomized into treatment groups (n = 10 mice/group) and administered **11b** orally (100 μL/dose) at the doses indicated and relative tumor volume to those at day 1 of treatment with **11b** measured as defined in the Experimental Section. Statistical analyses for efficacy of **11b** are detailed in Table 5.

Table 4. Effects of 11 b in the U251 MG Human Glioblastoma Model

		% incidence of tumor regressions		
treatment	dose	partial/ stasis	complete	% maximum tumor growth inhibition vs vehicle control
11b (p.o. bid)	1 mg/kg	0	0	43% NS
	3 mg/kg	0	0	61% $p < 0.01$
	10 mg/kg	20%	0	75% $p < 0.001$
	30 mg/kg	44%	0	88% $p < 0.001$

Table 5. Effects of 11b in the A375 Human Melanoma Model

		% incidence of tumor regressions		
treatment	dose	partial/ stasis	complete	% maximum tumor growth inhibition vs vehicle control
11b (p.o. bid)	0.3 mg/kg	20%	10%	71% $p < 0.05$
	1 mg/kg	10%	20%	73% $p < 0.01$
	3 mg/kg	11%	22%	90% $p < 0.001$
	10 mg/kg	50%	40%	98% $p < 0.001$

plasma and tumor levels of **11b** were 456 ± 44 ng/mL and 140 ± 20 ng/g, respectively. Administration of **11b** was well-tolerated, with no apparent toxicity or significant body weight loss or morbidity in solid tumor-bearing animals.

Compound **11b** was further evaluated in the P388 murine leukemia model to assess effects of varying dose schedules on survival in a systemic hematological tumor model. An improvement in median survival was observed at 30 mg/kg

dx.doi.org/10.1021/jm201449n | J. Med. Chem. 2012, 55, 903−913

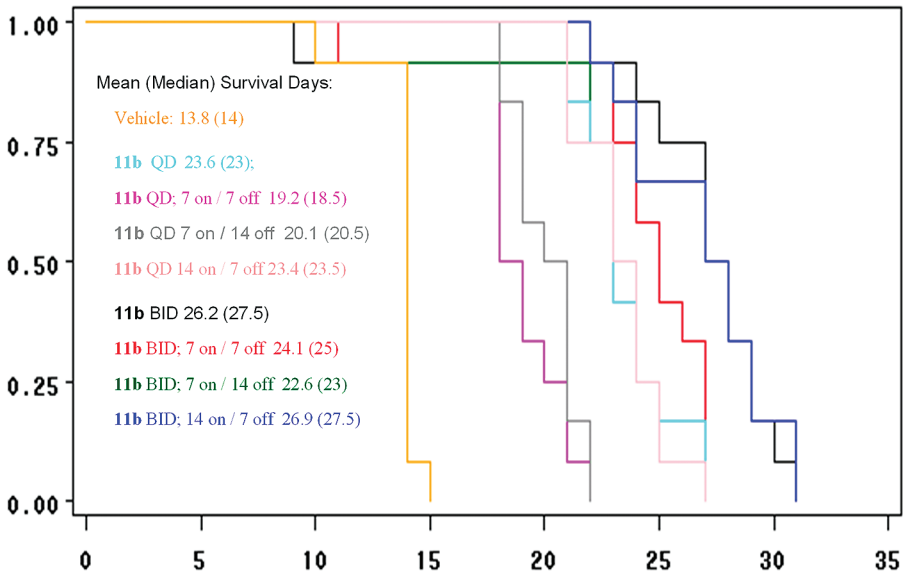

Figure 7. Survival benefit of continuous and intermittent oral administration of **11b** in the P388 systemic murine leukemia model in mice. Kaplan–Meier survival plot of continuous versus intermittent once and twice daily oral dosing regimens of **11b** (30 mg/kg po) on median survival of DBA/2 mice implanted with murine P388 leukemia cells. Details of analyses are defined in the Experimental Section and the text.

bid monotherapy in P388 leukemic DBA/2 mice relative to vehicle-treated tumor-bearing mice. Both continuous bid and qd oral administration and all intermittent oral dosing regimens bid and qd evaluated at 30 mg/kg in leukemic mice conferred sustained improvements in median survival ($p < 0.05$ or greater) relative to that of vehicle-treated leukemic animals. Survival data generated by Kaplan–Meier analyses for continuous and intermittent bid and qd administration of **11b** in the murine P388 leukemia ascite model in DBA/2 mice are shown in Figure 7.

CONCLUSIONS

Compound **11b** was identified as a potent, orally active inhibitor of human TIE-2, VEGF-R1 and 2, and FGF-R1. Collectively, it exhibits excellent permeability, metabolic stability and pharmacokinetic properties across multiple species and was advanced into full development. The in vitro, ex vivo, and in vivo pharmacologic activities conducted across a panel of angiogenesis assays and subcutaneous and orthotopic rodent and human tumor models demonstrated sustained and concentration (dose) related antiangiogenic and antitumor efficacy (tumor growth inhibition, tumor regressions, and survival benefits) consistent with a potent TIE-2/VEGF-R1, R2 inhibitor with a broader kinase inhibitory profile. Clinical phase I studies assessing the safety and pharmacokinetics of **11b** have been completed and are the subject of a separate publication. Nonetheless, these clinical studies indicate linear, dose related increases in plasma pharmacokinetic exposure (mean C_{max} and AUC) with oral administration of **11b** at doses of 3.0 to 126 mg/m^2 and an oral half-life of 8–15 h on a 28 day once daily treatment cycle, with a 14 day treatment free period. Further, exposure-related increases in VEGF-R2 inhibition ex vivo were demonstrated with **11b** in a human plasma-based cellular bioassay using the rTRK-A-human/VEGF-R2 chimeric endothelial cells described in this article. Normalized cellular VEGF-R2 inhibition greater than 90% in select patient plasma samples from the phase 1 study was observed, especially in the 73, 97.4, and 126.6 mg/m^2 dosing cohorts, suggestive of molecular target-directed biological activity of **11b** in humans (data not shown). Phase 2 proof-of-concept studies with **11b** are planned in select genotyped cancer patient populations to fully assess the therapeutic potential of this novel kinase inhibitor.

EXPERIMENTAL SECTION

Chemistry. All reagents and anhydrous solvents were obtained from commercial sources and used as received. ^{1}H NMRs were obtained at 400 MHz in the solvent indicated with tetramethylsilane as an internal standard. Coupling constants (J) are in Hertz (Hz). Compounds were purified by normal phase flash silica gel chromatography or automated silica gel chromatography on a Combi-Flash Companion (ISCO, Inc.) monitored at 254 and 290 nm detection. Preparative TLC was run using Silica Gel GF 20 × 20 cm × 1000 μm plates (Analtech). Liquid chromatography–mass spectrometry (LC/MS) were obtained on a Bruker Esquire 2000 ion trap LCMS with the Agilent 1100 HPLC equipped with an Agilent Eclipse XDB-C8 2 × 30 cm 3.5 μm column. All final compounds tested in Table 1 had purity >96% determined by High Pressure Liquid Chromatography (HPLC) using a Zorbax RX-C8, 5 × 150 mm column eluting with a mixture of acetonitrile and water containing 0.1% trifluoroacetic acid with a gradient of 10–100%.

5-Cyano-11,12-dihydro-2-methyl-10-propyl-indazolo[5,4-a]-carbazole-4-carboxylic Acid Ethyl Ester (8a). 5-Cyano-2,10,11,12-tetrahydro-2-methyl-indazolo[5,4-*a*]carbazole-4-carboxylic acid ethyl ester **7** (1.0 g, 2.7 mmol), 10 N NaOH (10 mL), and 1-iodopropane (2.7 mL, 27.0 mmol) in acetone (35 mL) was stirred at reflux overnight. The reaction was concentrated, triturated with water, and collected. The product was purified by flash chromatography (1% methanol in DCM) to afford 1.0 g (90%) as a tan solid. ^{1}H NMR (DMSO-d_6) δ: 8.44 (m, 1H), 7.80 (m, 1H), 7.64 (s, 1H), 7.62 (m, 1H), 7.36 (m, 1H), 4.59 (m, 2H), 4.52 (m, 2H), 3.87 (s, 3H), 3.53 (m, 2H), 2.88 (m, 2H), 1.83 (m, 2H), 1.37 (m, 3H), 0.91 (m, 3H). LCMS m/z: 413 (M + 1).

The intermediates **8b** and **8c** were synthesized from **7** using the method for **8a**.

5-Cyano-11,12-dihydro-2-methyl-10-(2-methylpropyl)-indazolo[5,4-*a*]carbazole-4-carboxylic Acid Ethyl Ester (8b). ^{1}HNMR (DMSO-d_6) δ: 8.45 (m, 1H), 7.84 (m, 1H), 7.64 (s, 1H), 7.62 (m, 1H), 7.35 (m, 1H), 4.52 (m, 4H), 3.87 (s, 3H), 3.51 (m, 2H), 2.87 (m, 2H), 1.37 (m, 4H), 0.80 (d, 6H, J = 7 Hz); LCMS m/z: 427 (M + 1).

dx.doi.org/10.1021/jm201449n | J. Med. Chem. 2012, 55, 903–913

5-Cyano-11,12-dihydro-2-methyl-10-(1-methylethyl)-indazolo[5,4-*a*]carbazole-4-carboxylic Acid Ethyl Ester (8c). ^{1}H NMR (DMSO-d_6) δ: 8.44 (d, 1H, J = 8 Hz), 7.92 (d, 1H, J = 9 Hz), 7.66 (s, 1H), 7.57 (m, 1H), 7.36 (m, 1H), 5.27 (m, 1H), 4.51 (m, 2H), 3.87 (s, 3H), 3.48 (m, 2H), 2.82 (m, 2H), 1.63 (d, 6H, J = 7 Hz), 1.39 (m, 3H). LCMS m/z: 413 (M + 1).

11-Propyl-11,12-dihydro-2-methyl-8-amino-4*H*-indazolo-[5,4-*a*]pyrrolo[3,4-*c*]carbazol-4-one (10a). To **8a** (800 mg, 1.94 mmol) in acetic acid (70 mL) was added dropwise 70% nitric acid (248 μL, 3.88 mmol). The reaction was heated at 80 °C for 1 h and then cooled to rt. The resulting precipitate was collected by filtration and washed with water, ether, and then dried. The crude nitro intermediate was dissolved in DMF−MeOH (30 mL, 1:1) and hydrogenated with excess Raney-Ni at 50 psi for 16 h on a Parr apparatus. The catalyst was removed by filtration through a bed of Celite, and the filtrate was concentrated under reduced pressure and dried to give **10a** (529 mg, 71%) as a tan solid. ^{1}H NMR (DMSO-d_6) δ: 8.83 (s, 1H), 8.30 (s, 1H), 7.37 (d, 1H, J = 9 Hz), 7.07 (s, 1H), 6.84 (d, 1H, J = 9 Hz), 4.82 (s, 2H), 4.67 (s, 2H), 4.43 (m, 2H), 3.85 (s, 3H), 3.41 (m, 2H), 2.82 (m, 2H), 1.77 (m, 2H), 0.88 (m, 3H). LCMS m/z: 386 (M + 1).

The intermediates **10b** and **10c** were synthesized from **8b** and **8c** using the method for **10a**.

11-(2-Methylpropyl)-12,13-dihydro-2-methyl-8-amino-4*H*-indazolo[5,4-*a*]pyrrolo[3,4-*c*]carbazol-4-one (10b). ^{1}H NMR (DMSO-d_6) δ: 8.84 (s, 1H), 8.31 (s, 1H), 7.39 (m, 1H), 7.06 (m, 1H), 6.82 (m, 1H), 4.82 (s, 2H), 4.68 (s, 2H), 4.34 (m, 2H), 3.85 (s, 3H), 3.38 (m, 2H), 2.80 (m, 2H), 2.07 (m, 1H), 0.77 (d, 6H, J = 7 Hz). LCMS m/z: 400 (M + 1).

11-(1-Methylethyl)-12,13-dihydro-2-methyl-8-amino-4*H*-indazolo[5,4-*a*]pyrrolo[3,4-*c*]carbazol-4-one (10c). ^{1}H NMR (DMSO-d_6) δ: 8.81 (s, 1H), 8.30 (s, 1H), 7.49 (d, 1H), 7.19 (s, 1H), 6.78 (d, 1H), 5.12 (m, 1H), 4.84 (s, 2H), 4.71 (s, 2H), 3.85 (s, 3H), 3.36 (m, 2H), 2.78 (m, 2H), 1.54 (d, 6H, J = 7 Hz); LCMS m/z: 386 (M + 1).

11-Propyl-12,13-dihydro-2-methyl-8-(pyrimidin-2-ylamino)-4*H*-indazolo[5,4-*a*]pyrrolo[3,4-*c*]carbazol-4-one (11a). Intermediate **9a** (1.0 g, 2.6 mmol) and 2-chloropyrimidine (390 mg, 3.4 mmol) in 1-butanol (35 mL) were heated at reflux for 24 h. The mixture was then cooled to rt and concentrated under vacuum. The product was purified using silica gel column chromatography (9% MeOH in DCM) to give **11a** as a tan solid (633 mg, 53%). Purity 99%. ^{1}H NMR (DMSO-d_6) δ: 9.55 (s, 1H), 8.86 (s, 1H), 8.47 (m, 2H), 8.36 (s, 1H), 8.29 (m, 1H), 7.81 (m, 1H), 7.61 (m, 1H), 6.79 (m, 1H), 4.74 (s, 2H), 4.53 (m, 2H), 3.87 (s, 3H), 3.46 (m, 2H), 2.84 (m, 2H), 1.82 (m, 2H), 0.90 (m, 3H). LCMS m/z: 464 (M + H).

Compounds **11b**−**11j** were synthesized using the method for **11a**.

11-(2-Methylpropyl)-12,13-dihydro-2-methyl-8-(pyrimidin-2-ylamino)-4*H*-indazolo[5,4-*a*]pyrrolo[3,4-*c*]carbazol-4-one (11b). ^{1}H NMR (DMSO-d_6) δ: 9.57 (s, 1H), 8.87 (s, 1H), 8.47 (m, 2H), 8.40 (s, 1H), 8.29 (m, 1H), 7.81 (m, 1H), 7.64 (m, 1H), 6.80 (m, 1H), 4.75 (s, 2H), 4.43 (m, 2H), 3.87 (s, 3H), 3.43 (m, 2H), 2.83 (m, 2H), 2.12 (m, 1H), 0.80 (d, 6H, J = 7 Hz). LCMS m/z 478 (M + 1).

11-(1-Methylethyl)-12,13-dihydro-2-methyl-8-(pyrimidin-2-ylamino)-4*H*-indazolo[5,4-*a*]pyrrolo[3,4-*c*]carbazol-4-one (11c). ^{1}H NMR (DMSO-d_6) δ: 9.56 (s, 1H), 8.78 (s, 1H), 8.47 (d, 2H, J = 5 Hz), 8.36 (s, 1H), 8.28 (s, 1H), 7.78 (m, 2H), 6.81 (t, 1H, J = 5 Hz), 5.23 (m, 1H), 4.73 (s, 2H), 3.93 (s, 3H), 3.39 (m, 2H), 2.81 (m, 2H), 1.61 (d, 6H, J = 7 Hz). LCMS m/z: 464 (M + 1).

11-Propyl-12,13-dihydro-2-methyl-8-(5-ethyl-pyrimidin-2-ylamino)-4*H*-indazolo[5,4-*a*]pyrrolo[3,4-*c*]carbazol-4-one (11d). ^{1}H NMR (DMSO-d_6) δ: 9.44 (s, 1H), 8.85 (s, 1H), 8.37 (s, 3H), 8.31 (m, 1H), 7.80 (m, 1H), 7.59 (m, 1H), 4.74 (s, 2H), 4.54 (m, 2H), 3.87 (s, 3H), 3.46 (m, 3H), 2.84 (m, 2H), 2.50 (m, 2H), 1.83 (m, 1H), 1.19 (m, 3H), 0.90 (m, 3H). LCMS m/z: 492 (M + 1).

11-(2-Methylpropyl)-12,13-dihydro-2-methyl-8-(5-ethylpyrimidin-2-ylamino)-4*H*-indazolo[5,4-*a*]pyrrolo[3,4-*c*]carbazol-4-one (11e). ^{1}H NMR (DMSO-d_6) δ: 9.43 (s, 1H), 8.86 (s, 1H), 8.37 (s, 3H), 8.31 (s, 1H), 7.79 (m, 1H), 7.62 (m, 1H), 4.75 (s, 2H), 4.43 (m, 2H), 3.87 (s, 3H), 3.43 (m, 2H), 2.83 (m, 2H), 2.50 (m, 2H), 2.12 (m, 1H), 1.19 (m, 3H), 0.80 (d, 6H, J = 7 Hz). LCMS m/z: 506 (M + 1).

11-(2-Methylpropyl)-12,13-dihydro-2-methyl-8-(4,6-dimethylpyrimidin-2-ylamino)-4*H*-indazolo[5,4-*a*]pyrrolo[3,4-*c*]-carbazol-4-one (11f). ^{1}H NMR (DMSO-d_6) δ: 9.50 (s, 1H), 8.86 (s, 1H), 8.69 (m, 1H), 8.37 (s, 1H), 7.70 (m, 1H), 7.61 (m, 1H), 6.62 (s, 1H), 4.77 (s, 2H), 4.43 (m, 2H), 3.86 (s, 3H), 3.40 (m, 2H), 2.82 (m, 2H), 2.36 (s, 6H), 2.12 (m, 1H), 0.80 (d, 6H, J = 7 Hz). LCMS m/z: 506 (M + 1).

11-(2-Methylpropyl)-12,13-dihydro-2-methyl-8-(4-methoxy-pyrimidin-2-ylamino)-4*H*-indazolo[5,4-*a*]pyrrolo[3,4-*c*]-carbazol-4-one (11g). ^{1}H NMR (DMSO-d_6) δ: 9.50 (s, 1H), 8.86 (s, 1H), 8.35 (m, 2H), 8.20 (m, 1H), 7.80 (m, 1H), 7.65 (m, 1H), 6.25 (m, 1H), 4.75 (s, 2H), 4.43 (m, 2H), 3.98 (s, 3H), 3.86 (s, 3H), 3.43 (m, 2H), 2.83 (m, 2H), 2.57 (m, 1H), 0.80 (d, 6H, J = 7 Hz). LCMS m/z: 508 (M + 1).

11-(2-Methylpropyl)-12,13-dihydro-2-methyl-8-(4-trifluoro-methyl-pyrimidin-2-ylamino)-4*H*-indazolo[5,4-*a*]pyrrolo[3,4-*c*]carbazol-4-one (11h). ^{1}H NMR (DMSO-d_6) δ: 10.23 (s, 1H), 8.87 (s, 1H), 8.81 (m, 1H), 8.45 (m, 2H), 7.70 (s, 2H), 7.23 (m, 1H), 4.74 (s, 2H), 4.45 (m, 2H), 3.87 (s, 3H), 3.43 (m, 2H), 2.83 (m, 2H), 2.13 (m, 1H), 0.81 (d, 6H, J = 7 Hz). LCMS m/z: 546 (M + 1).

11-(2-Methylethyl)-12,13-dihydro-2-methyl-8-(3-pyridazinylamino)-4*H*-indazolo[5,4-*a*]pyrrolo[3,4-*c*]carbazol-4-one (11i). ^{1}H NMR (DMSO-d_6) δ: 9.26 (s, 1H), 8.78 (s, 1H), 8.63 (m, 1H), 8.38 (m, 1H), 8.30 (m, 1H), 7.77 (m, 1H), 7.70 (m, 1H), 7.45 (m, 1H), 7.15 (m, 1H), 5.23 (m, 1H), 4.73 (s, 2H), 3.93 (s, 3H), 3.39 (m, 2H), 2.81 (m, 2H), 1.62 (d, 6H, J = 7 Hz); LCMS m/z: 464 (M + 1).

11-(2-Methylethyl)-12,13-dihydro-2-methyl-8-(4-pyridinylamino)-4*H*-indazolo[5,4-*a*]pyrrolo[3,4-*c*]carbazol-4-one (11j). ^{1}H NMR (DMSO-d_6) δ: 9.26 (s, 1H), 8.83 (s, 1H), 8.78 (s, 1H), 8.37 (s, 1H), 8.16 (m, 2H), 7.82 (d, 1H, J = 8 Hz), 7.68 (m, 1H), 7.29 (m, 1H), 6.89 (m, 2H), 5.30 (m, 1H), 4.75 (s, 2H), 3.86 (s, 3H), 3.41 (m, 2H), 2.79 (m, 2H), 1.62 (d, 6H, J = 7 Hz). LCMS m/z: 463 (M + 1).

5-Cyano-11,12-dihydro-1-methyl-10-(2-methylpropyl)-indazolo[5,4-*a*]carbazole-4-carboxylic acid ethyl ester (13). This compound was synthesized from intermediate **12** using the method for **8a**. LCMS m/z: 427 (M + 1).

11-(2-Methylpropyl)-12,13-dihydro-1-methyl-8-amino-4*H*-indazolo[5,4-*a*]pyrrolo[3,4-*c*]carbazol-4-one (14). This compound was synthesized from **13** using the method for **10a**; tan solid. LCMS m/z: 400 (M + H).

11-(2-Methylpropyl)-12,13-dihydro-1-methyl-8-(pyrimidin-2-ylamino)-4*H*-indazolo[5,4-*a*]pyrrolo[3,4-*c*]carbazol-4-one (15). This compound was synthesized from **14** using the method for **11a**. ^{1}H NMR (DMSO-d_6) δ: 9.55 (s, 1H), 8.75 (s, 1H), 8.47 (d, 2H, J = 5 Hz), 8.32 (s, 1H), 8.30 (s, 1H), 7.81 (m, 1H), 7.63 (d, 1H, J = 9 Hz), 6.81 (t, 1H, J = 5 Hz), 4.75 (s, 2H), 4.44 (d, 2H, J = 7 Hz), 3.81 (s, 3H), 3.48 (t, 2H, J = 7 Hz), 2.97 (t, 2H, J = 7 Hz), 2.12 (m, 1H), 0.81 (d, 6H, J = 7 Hz). LCMS m/z: 478 (M + 1).

VEGF-R2 and TIE-2 Kinase Assays. Compounds were tested for their ability to inhibit the kinase activity of baculovirus-expressed cytoplasmic domain of VEGF-R2 or TIE-2 using the TRF detection system. Briefly, each 96-well Costar high binding plate (Corning Costar #3922, Corning, NY) was coated with 100 μL/well of 10 μg/mL substrate solution (recombinant GST-PLCγ) in Tris-buffered saline (TBS). The kinase reaction mixture (total volume = 100 μL/well) consisting of 20 mM HEPES, pH 7.2, 40 μM ATP, 10 mM $MnCl_2$, 0.1% bovine serum albumin (BSA), and test compound (diluted in DMSO; 2.5% DMSO final in assay) was then added to the assay plate. Enzyme (30 ng/mL VEGF-R2 or 200 ng/mL TIE-2) was added, and the reaction was allowed to proceed at 37 °C for 15 min. Detection of the phosphorylated product was performed by adding 100 μL/well of Eu−N1 labeled PY100 antibody (PerkinElmer # AD0160, Boston, MA) diluted 1:5,000 in TBS-T containing 0.25% BSA). Incubation at 37 °C then proceeded for 1 h, followed by the addition of 100 μL of enhancement solution (PerkinElmer #1244-105). The plate was gently agitated, and after 30 min, the fluorescence of the resulting solution was measured using the PerkinElmer EnVision 2100 (or 2102) multilabel plate reader. Inhibition curves for compounds were generated by plotting percent control activity

dx.doi.org/10.1021/jm201449n | J. Med. Chem. 2012, 55, 903−913

versus $\log_{10}$ of the concentration of compound. IC_{50} values were calculated by nonlinear regression using the sigmoidal dose−response (variable slope) equation in GraphPad Prism as follows:

$$y = \text{bottom} + (\text{top} - \text{bottom})/(1 + 10(\log IC_{50} - x) \times \text{Hill slope})$$

where y is the % kinase activity at a given concentration of compound, x is the logarithm of the concentration of compound, bottom is the % of control kinase activity at the highest compound concentration tested, and top is the % of control kinase activity at the lowest compound concentration examined. The values for bottom and top were fixed at 0 and 100, respectively. IC_{50} values were reported as the average of two or more separate determinations.

VEGF-R2 Cellular Assay. The porcine aortic endothelial cell line (PAE 145) stably transfected with chimeric rTRK-A/KDR receptor containing the extracellular domain of rat TRK-A and the intracellular domain of human VEGF-R2 was used for this study. Subconfluent cells were serum-starved by replacing media with 5 mL of serum-free DMEM (Cellgro 10-013-CM; Mediatech, Inc., Herndon, VA) containing 0.05% BSA for 1 h at 37 °C. At the same time, test compound (various concentrations) or DMSO (control) was added to the cells (0.1% final DMSO in assay). To induce phosphorylation, cells were treated with nerve growth factor (NGF; Harlan Bioproducts for Science, Inc. BT-5017; Indianapolis, IN) at a concentration of 10 ng/mL for 5 min. Cells were lysed in FRAK buffer (10 mM Tris at pH 7.5, 50 mM NaCl, 1% Triton X-100, 20 mM NaF, 2 mM sodium pyrophosphate, 0.1% BSA, and 25 mM β-glycerophosphate) containing 1 mM activated sodium vanadate and protease inhibitors (Protease Inhibitor Cocktail Set III Calbiochem # 539134; San Diego, CA) sheared with a 27-gauge syringe, then centrifuged at 12,000g for 15 min at 4 °C. Clarified cell lysates were normalized to protein using the bicinchoninic acid (BCA; Pierce # 23235; Rockford, IL) method, immunoprecipitated with anti-VEGF-R2 antibody (CEP-133) for 1 h, followed by incubation with Protein A Sepharose (Sigma # P3391; St. Louis, MO) for another hour at 4 °C. Immunoprecipitates were washed three times with FRAK buffer containing protease/phosphatase inhibitors, 4× sample buffer was added, and then heated for 5 min at 85 °C. Samples were processed using the standard protocol involving gel separation (NuPAGE 3−8% Tris-acetate gel; NOVEX # EA-03585; Invitrogen, Carlsbad, CA) and transfer to nitrocellulose membrane. The membranes were blocked with Blocking Buffer (LiCor #927−40000; Lincoln, NE) overnight, then immunoblotted with 4G10 antiphosphotyrosine antibody, followed by incubation with Alexa Fluor 680 goat antimouse IgG (Molecular Probes #A-21058; Eugene, OR) at RT for 1 h. Phosphorylated proteins were visualized by scanning on the Odyssey Infrared Imaging System (LiCor). Inhibition of phosphorylation was calculated with the help of the Gel-Pro Analyzer 3.1 software (Fotodyne, Inc.; Hartland, WI).

TIE-2 Cellular Assay. The TIE-2 cell-based assay was performed as described above for VEGF-R2 except that the PAE 145 cell line stably transfected with chimeric rTRK-A/TIE-2 receptor containing the extracellular domain of rat TRK-A, and the intracellular domain of human TIE-2 was used.

Rat Pharmacokinetics. Adult male Sprague−Dawley rats (275−350 g; Charles River, Kingston, New York) and male cynomolgus monkeys (2−4 kg, Covance Laboratories, Alice TX) were used in the experiments. All animal usage was approved by the Cephalon IACAC. For routine compound screening, rats were dosed via the lateral tail vein at the indicated dose for i.v. administration (3% DMSO, 30% solutol, 67% phosphate buffered saline) or via oral gavage (0.6% methylcellulose/Tween 80 (99.5:0.5) or Ora Plus) at the indicated dose. Rats were fasted overnight prior to p.o. administration. Serial blood samples were collected from the lateral tail vein into heparinized collection tubes (approximately 0.25 mL) at 7 sampling times over a 6 h or a 24 h period as indicated. The plasma was separated by centrifugation, and the sample was prepared for HPLC/MS analysis by protein precipitation with acetonitrile. The plasma samples were analyzed for drug and internal standard via LC-MS/MS protocol. The pharmacokinetic parameters were calculated by a noncompartmental method using WinNonlin software (Professional Version 4.1, Pharsight Corporation, Palo Alto, CA, 1997). For experiments to determine detailed rat PK parameters, rats were administered 1 mg/kg i.v. and 3 mg/kg p.o. in saline and parameters calculated from composite mean plasma concentration−time data (n = 12). Monkey PK (0.5 mg/kg i.v.; 47.4% polyethylene glycol (PEG) 400; 31.1% water; 20.7% hydroxyl-β-cyclodextrin (HPBCD); and 0.8% Pluronic F-68 and p.o. Three mg/kg; Ora Plus) parameters calculated using plasma concentration−time data for individual animals (monkey n = 4).

In Vitro Capillary Tube Formation Assay with HUVECs on Matrigel and Ex Vivo Rat Aortic Ring Explant Assay in Collagen Gel Matrices. The ability of **11b** to inhibit angiogenesis in vitro in a capillary tube formation assay utilizing human umbilical vein endothelial cells (HUVECs) cultured on a synthetic basement membrane matrix and ex vivo in rat aortic ring explant cultures was conducted using published methods.[17]

A375 Melanoma and U251 MG Glioblastoma Sc Xenograft Models. Tumor cells were obtained from the American Type Culture Collection (Manassas, VA) and cultured to subconfluency in RPMI1620 medium with 10% FBS. Harvested cells (5×10^6) were injected subcutaneously in serum-free media into the right flank of athymic female nude mice (Charles River). Twelve days post-implantation, mice with established tumors (approximately 60−100 mm^3) were randomized into treatment groups (n = 10 mice/group) and administered **11b** bid (100 μL/dose) at doses of 0.3 mg/kg, 1 mg/kg, 3 mg/kg, 10 mg/kg, and 30 mg/kg depending upon the specific model in an oral suspension of methylcellulose−Tween (Ora-Plus). Tumor volumes were determined every 3−5 days using vernier calipers and the formula: V (mm^3) = 0.5236 × length (mm) × width (mm) [length (mm + width (mm)/2]. Relative tumor volumes to that at the start of treatment were calculated for the A375 melanoma model. Statistical analyses of changes in tumor volume (or relative tumor volume) with **11b** treatment were done using the Mann−Whitney Rank Sum test, with $p < 0.05$ deemed significant.

P388 Murine Leukemia Model. P388 murine leukemia cells were obtained from the American Type Culture Collection (Manassas, VA) and cultured in suspension in RPMI1620 medium with 10% FBS. At approximately 6 weeks of age, female DBA/2 mice (Charles River) were implanted intraperitoneally with leukemic cells and the resultant ascites isolated and serially passaged in DBA/2 mice for three cycles to generate highly malignant leukemic clones for subsequent evaluation in efficacy studies. Upon intraperitoneal implantation of ascitic P388 leukemia cells into DBA/2 mice, animals were randomized into treatment groups (n = 12 mice/group) to receive **11b** orally at a 30 mg/kg dose in methylcellulose: Tween vehicle on four distinct continuous and alternate dosing schedules, bid continuous; qd continuous; bid and qd × 7 days followed by drug holiday × 7 days; bid and qd × 14 days followed by drug holiday × 7 days; bid and qd × 7 days followed by drug holiday × 14 days. Mice were weighed twice weekly and monitored daily. The effects of **11b** on the survival of tumor bearing mice were analyzed by the Kaplan−Meier method as required for data sets using SAS (SAS 8.2, SAS Institute, Inc. Cary, NC). Mann−Whitney Rank Sum test analyses were used to compare mean and median survival times and body weights between treatment groups.

AUTHOR INFORMATION

Corresponding Author

*Phone: 610-738-6283. Fax: 610-738-6558. E-mail: rhudkins@cephalon.com or Robert.Hudkins@tevapharm.com.

ABBREVIATIONS

VEGF-R, vascular endothelial growth factor receptor kinase; TIE-2, tyrosine kinase with immunoglobulin and EGF-like domains 2; FGF-R, fibroblast growth factor receptor; DHI, N2-methyl-12,13-dihydroindazolo[5,4-a]pyrrolo[3,4-c]carbazole; HUVEC, primary human umbilical vein endothelial cells; KDR,

kinase insert domain receptor; RTK, receptor tyrosine kinase; PDGF-R, platelet-derived growth factor receptor; TRF, heterogeneous time-resolved fluorescence; GST, human phospholipase C-γ/glutathione *S*-transferase; PK, pharmacokinetics; TRK-A, neurotrophic tyrosine kinase receptor type 1; BAEC, bovine aortic endothelial cells; HMVEC, human dermal microvascular endothelial cells

REFERENCES

(1) (a) Folkman, J. Tumor angiogenesis: therapeutic implications. *N. Engl. J. Med.* **1971**, *285*, 1182−1186. (b) Folkman, J.; Shing, Y. Angiogenesis. *J. Biol. Chem.* **1992**, *267*, 10931−10934. (c) Carmeliet, P.; Jain, R. K. Angiogenesis in cancer and other diseases. *Nature* **2000**, *407*, 249−257;(d) Folkman, Angiogenesis in cancer, vascular, rheumatoid and other disease. *J. Nat. Med.* **1995**, *1*, 27−31.

(2) Hurwitz, H.; Fehrenbacher, L.; Novotny, W.; Cartwright, T.; Hainsworth, J.; Heim, W.; Berlin, J.; Baron, A.; Griffing, S.; Holmgren, E.; Ferrara, N.; Fyfe, G.; Rogers, B.; Ross, R.; Kabbinavar, F. Bevacizumab plus irinotecan, fluorouracil, and leucovorin for metastatic colorectal cancer. *N. Engl J. Med.* **2004**, *350*, 2335−2342.

(3) Escudier, B.; Eisen, T.; Stadler, W. M.; Szczylik, C.; Oudard, S.; Staehler, M.; Negrier, S.; Chevreau, C.; Desai, A. A.; Rolland, F.; Demkow, T.; Hutson, T. E.; Gore, M.; Anderson, S.; Hofilena, G.; Shan, M.; Pena, C.; Lathia, C.; Bukowski, R. M. Sorafenib for treatment of renal cell carcinoma: Final efficacy and safety results of the phase III treatment approaches in renal cancer global evaluation trial. *J. Clin. Oncol.* **2009**, *27*, 3312−3318.

(4) Demetri, G. D.; van Oosterom, A. T.; Garrett, C. R.; Blackstein, M. E.; Shah, M. H.; Verweij, J.; McArthur, G.; Judson, I. R.; Heinrich, M. C.; Morgan, J. A.; Desai, J.; Fletcher, C. D.; George, S.; Bello, C. L.; Huang, X.; Baum, C. M.; Casali, P. G. Efficacy and safety of sunitinib in patients with advanced gastrointestinal stromal tumour after failure of imatinib: a randomised controlled trial. *Lancet* **2006**, *368*, 1329−1338.

(5) (a) Xu, C. F.; Bing, N. X.; Ball, H. A.; Rajagopalan, D.; Sternberg, C. N.; Hutson, T. E.; de Souza, P.; Xue, Z. G.; McCann, L.; King, K. S.; Ragone, L. J.; Whittaker, J. C.; Spraggs, C. F.; Cardon, L. R.; Mooser, V. E.; Pandite, L. N. Pazopanib efficacy in renal cell carcinoma: Evidence for predictive genetic markers in angiogenesis-related and exposure-related genes. *J. Clin. Oncol.* **2011**, *29*, 2557−2564. (b) Harris, P. A.; Boloor, A.; Cheung, M.; Kumar, R.; Crosby, R. M.; Davis-Ward, R. G.; Epperly, A. H.; Hinkle, K. W.; Hunter, R. N. III; Johnson, J. H.; Knick, V. B.; Laudeman, C. P.; Luttrell, D. K.; Mook, R. A.; Nolte, R. T.; Rudolph, S. K.; Szewczyk, J. R.; Truesdale, A. T.; Veal, J. M.; Wang, L.; Stafford, J. A. Discovery of 5-[[4-[(2,3-dimethyl-2H-indazol-6-yl)methylamino]-2-pyrimidinyl]amino]-2-methyl-benzenesulfonamide (Pazopanib), a novel and potent vascular endothelial growth factor receptor inhibitor. *J. Med. Chem.* **2008**, *51*, 4632−4640.

(6) Cai, Z. W.; Zhang, Y.; Borzilleri, R. M.; Qian, L.; Barbosa, S.; Wei, D.; Zheng, X.; Wu, L.; Fan, J.; Shi, Z.; Wautlet, B. S.; Mortillo, S.; Jeyaseelan, R. Sr; Kukral, D. W.; Kamath, A.; Marathe, P.; D'Arienzo, C.; Derbin, G.; Barrish, J. C.; Robl, J. A.; Hunt, J. T.; Lombardo, L. J.; Fargnoli, J.; Bhide, R. S. Discovery of brivanib alaninate ((S)-((R)-1-(4-(4-fluoro-2-methyl-1H-indol-5-yloxy)-5-methylpyrrolo[2,1-f]-[1,2,4]triazin-6-yloxy)propan-2-yl)2-aminopropanoate), a novel pro-drug of dual vascular endothelial growth factor receptor-2 and fibroblast growth factor receptor-1 kinase inhibitor (BMS-540215). *J. Med. Chem.* **2008**, *51*, 1976−1980.

(7) Bergers, G.; Benjamin, L. E. Tumorigenesis and the angiogenic switch. *Nat. Rev. Cancer* **2003**, *3*, 401−410.

(8) (a) Lin, P.; Buxton, J. A.; Acheson, A.; Radziejewski, C.; Maisonpierre, P. C.; Yancopoulos, G. D.; Channon, K. M.; Hale, L. P.; Dewhirst, M. W.; George, S. E.; Peters, K. G. Antiangiogenic gene therapy targeting the endothelium-specific receptor tyrosine kinase TIE-2. *Proc. Natl. Acad. Sci. U.S.A.* **1998**, *95*, 8829−8834. (b) Cristofanilli, M.; Charnsangavej, C.; Hortobagyi, G. N. Angiogenesis modulation in cancer research: novel clinical approaches. *Nat. Rev. Drug Discovery* **2002**, *1*, 415−426. (c) Jones, N.; LLjin, K.; Dumount, D.; Alitalo, K. TIE receptors: new modulators of angiogenic and lymphangiogenic responses. *Nat. Rev. Mol. Cell Biol.* **2001**, *2*, 257−267. (d) Uemura, A.; Ogawa, M.; Hirashima, M.; Fujiwara, T.; Koyama, S; Takagi, H.; Honda, Y.; Wiegand, S, J.; Yancopoulos, G. D.; Nishikawa, S. *J. Clin. Invest.* **2002**, *110*, 1619−1628. (e) Visconti, R. P.; Richardson, C. D.; Sato, T. N. Orchestration of angiogenesis and arteriovenous contribution by angiopoietins and vascular endothelial growth factor (VEGF). *Proc. Natl. Acad. Sci. U.S.A.* **2002**, *99*, 8219−8224. (f) Jain, R. K. Molecular regulation of vessel maturation. *Nature Med.* **2003**, *9*, 685−693.

(9) (a) Lin, P.; Polverini, P.; Dewhirst, M.; Shan, S.; Rao, P. S.; Peters, K. G. Inhibition of tumor angiogenesis using a soluble receptor establishes a role for TIE-2 in pathologic vascular growth. *J. Clin. Invest.* **1997**, *100*, 2072−2078. (b) Shim, W. S.; Teh, M.; Mack, P. O.; Ge, R. Inhibition of angiopoietin-1 expression in tumor cells by an antisense RNA approach inhibited xenograft tumor growth in immunodeficient mice. *Int. J. Cancer* **2001**, *94*, 6−15. (c) Stratmann, A.; Acker, T.; Burger, A. M.; Amann, K.; Risau, W.; Plate, K. H. Differential inhibition of tumor angiogenesis by TIE-2 and vascular endothelial growth factor receptor-2 dominant-negative receptor mutants. *Int. J. Cancer* **2001**, *91*, 273−282.

(10) (a) Jendreyko, N.; Popkov, M.; Rader, C.; Barbas, C. F. Phenotypic knockout of VEGF-R2 and TIE-2 with an intradiabody reduces tumor growth and angiogenesis in vivo. *Proc. Natl. Acad. Sci. U.S.A.* **2005**, *102*, 8293−8298. (b) Popkov, M.; Jendreyko, N.; McGavern, D. B.; Rader, C.; Barbas, C. F. Targeting tumor angiogenesis with adenovirus-delivered anti-TIE-2 intrabody. *Cancer Res.* **2005**, *65*, 972−991.

(11) (a) Beebe, J. S.; Jani, J. P.; Knauth, E.; Goodwin, P.; Higdon, C.; Rossi, A. M.; Emerson, E.; Finkelstein, M.; Floyd, E.; Harriman, S.; Atherton, J.; Hillerman, S.; Soderstrom, C.; Kou, K.; Gant, T.; Noe, M. C.; Foster, B.; Rastinejad, F.; Marx, M. A.; Schaeffer, T.; Whalen, P. M.; Roberts, W. G. Pharmacological characterization of CP-547,632, a novel vascular endothelial growth factor receptor-2 tyrosine kinase inhibitor for cancer therapy. *Cancer Res.* **2003**, *63*, 7301−7309. (b) Hasegawa, M.; Nishigaki, N.; Washio, Y.; Kano, K.; Harris, P. A.; Sato, H.; Mori, I.; West, R. I.; Shibahara, M.; Toyoda, H.; Wang, L.; Nolte, R. T.; Veal, J. M.; Cheung, M. Discovery of novel benzimidazoles as potent inhibitors of TIE-2 and VEGF-R2 tyrosine kinase receptors. *J. Med. Chem.* **2007**, *50*, 4453−4470. (c) Ji, Z.; Ahmed, A. A.; Albert, D. H.; Bouska, J. J.; Bousquet, P. F.; Cunha, G. A.; Diaz, G.; Glaser, K. B.; Guo, J.; Harris, C. M.; Li, J.; Marcotte, P. A.; Moskey, M. D.; Oie, T.; Pease, L.; Soni, N. B.; Stewart, K. D.; Davidsen, S. K.; Michaelides, M. R. *J. Med. Chem.* **2008**, *51*, 1231−1241. (d) Miyazaki, Y.; Tang, J.; Maeda, Y.; Nakano, M.; Wang, L.; Nolte, R. T.; Sato, H.; Sugai, M.; Okamoto, Y.; Truesdale, A. T.; Hassler, D. F.; Nartey, E. N.; Patrick, D. R.; Ho, M. L.; Ozawa, K. Orally active 4-amino-5-diarylurea-furo[2,3-d]pyrimidine derivatives as anti-angiogenic agent inhibiting VEGF-R2 and TIE-2. *Bioorg. Med. Chem. Lett.* **2007**, *17*, 1773−1778. (e) Miyazakia, Y.; Matsunagaa, S.; Tanga, J.; Maedaa, Y.; Nakanoa, M.; Philippea, R. J.; Shibaharaa, M.; Liub, W.; Satoa, H.; Wangb, L.; Nolteb, R. T. Novel 4-amino-furo[2,3-d]pyrimidines as TIE-2 and VEGF-R2 dual inhibitors. *Bioorg. Med. Chem. Lett.* **2005**, *15*, 2203−2207.

(12) (a) Gingrich, D. E.; Reddy, D. R.; Iqbal, M. A.; Singh, J.; Aimone, L. D.; Angeles, T. S.; Albom, M.; Yang, S.; Meyer, S.; Ator, M.; Robinson, C.; Ruggeri, B. A.; Dionne, C. A.; Vaught, J. L.; Mallamo, J. P.; Hudkins, R. L. A new class of potent VEGF receptor tyrosine kinase inhibitors: structure-activity relationships for a series of 9-alkoxymethyl-12-(3-hydroxypropyl)indeno[2,1-a]pyrrolo[3,4-c]-carbazole-5-ones and the identification of CEP-5214 and its dimethylglycine ester prodrug clinical candidate CEP-7055. *J. Med. Chem.* **2003**, *46*, 5375−5388. (b) Ruggeri, B.; Singh, J.; Gingrich, D.; Angeles, T.; Albom, M.; Chang, H.; Robinson, C.; Hunter, K.; Dobrzanski, P.; Jones-Bolin, S.; Aimone, L.; Klein-Szanto, A.; Herbert, J.-M.; Bono, F.; Schaeffer, P.; Casellas, P.; Bourie, B.; Pili, R.; Isaacs, J.; Ator, M.; Hudkins, R.; Vaught, J.; Mallamo, J.; Dionne, C. CEP-7055: A novel, orally-active pan inhibitor of vascular endothelial growth

factor receptor tyrosine kinases with potent anti-angiogenic activity and anti-tumor efficacy in pre-clinical models. *Cancer Res.* **2003**, *63*, 5978−5991.

(13) (a) Becknell, N.; Zulli, A. L.; Angeles, T. S.; Yang, S.; Albom, M.; Aimone, L. D.; Robinson, C.; Chang, H.; Hudkins, R. L. Novel C-3 N-urea, amide and carbamate dihydroindazolo[5,4-a]pyrrolo[3,4-c]carbazole analogs as potent TIE-2 and VEGF-R2 dual inhibitors. *Bioorg. Med. Chem. Lett.* **2006**, *16*, 5368−5372. (b) Underiner, T. L.; Ruggeri, B.; Aimone, L. A.; Albom, M.; Angeles, T.; Chang, H.; Hudkins, R. L.; Hunter, K.; Josef, K.; Robinson, C.; Weinberg, L.; Yang, S.; Zulli, A. TIE-2/VEGF-R2 SAR and in vitro activity of C3-acyl and C3-oxo fused pyrrolodihydroindazolo-carbazole analogs. *Bioorg. Med. Chem. Lett.* **2008**, *18*, 2368−2373. (c) Dandu, R.; Zulli, A. L.; Bacon, E. R.; Underiner, T. L.; Robinson, C.; Chang, H.; Miknyoczki, S.; Grobelny, J.; Ruggeri, B.; Yang, S.; Albom, M. S.; Angeles, T.; Aimone, L. A.; Hudkins, R. L. Design and synthesis of dihydroindazolo[5,4-a]pyrrolo[3,4-c]carbazole oximes as potent dual inhibitors of TIE-2 and VEGF-R2 receptor tyrosine kinases. *Bioorg. Med. Chem. Lett.* **2008**, *18*, 1916−1921. (d) Hudkins, R. L.; Zulli, A. L.; Underiner, T. L.; Angeles, T. S.; Aimone, L. D.; Meyer, S. L.; Pauletti, D.; Chang, H.; Fedorov, E. V.; Almo, S. C.; Fedorov, A. A.; Ruggeri, B. A. 8-THP-DHI Analogs as Potent Type I Dual TIE-2/VEGF-R2 receptor tyrosine kinase inhibitors. *Bioorg. Med. Chem. Lett.* **2010**, *20*, 3356−3360.

(14) (a) Tao, M.; Park, C-H; Josef, K. A.; Hudkins, R. L. Regiospecific synthesis of 12,13-dihydroindazolo[5,4-a]pyrrolo[3,4-c]carbazole-4-one. *J. Heterocyclic Chem.* **2009**, *46*, 1185−1189. (b) Reddy, D. R.; Tao, M.; Josef, K. A.; Bacon, E. R.; Hudkins, R. L. Regiospecific synthesis of 5-(1H-indol-2-yl)-1- and −2-methyl-6,7-dihydro-2H-indazole isomers. *J. Heterocyclic Chem.* **2007**, *44*, 437−440. (c) Josef, K. A.; Reddy, D.; Tao, M.; Hudkins, R. L. Structure determination of N-methyl-1,4,6,7-tetrahydro-5H-indazol-5-one. *J. Heterocyclic. Chem.* **2006**, *43*, 719−722. (d) Hudkins, R. L.; Zulli, A. L.; Reddy, D. R.; Gingrich, D. E.; Tao, M.; Becknell, N. C.; Diebold, J. L.; Underiner, T. L. Preparation of Novel Fusedpyrrolocarbazoles for Treating or Preventing Angiogenesis or Angiogenesis Disorders. US Patent US20050143442. (e) Hudkins, R. L.; Diebold, J. L.; Tao, M.; Josef, K. A.; Park, C. H.; Angeles, T. S.; Aimone, L. D.; Husten, J.; Ator, M. A.; Meyer, S. L.; Holskin, B. P.; Durkin, J. T.; Fedorov, A. A.; Fedorov, E. V.; Almo, S. C.; Mathiasen, J.; Bozyczko-Coyne, D.; Saporito, M. S.; Mallamo, J. P. Mixed lineage kinase 1 (MLK1) and mixed lineage kinase 3 (MLK3) subtype selective dihydronaphthyl-[3,4-a]pyrrolo[3,4-c]carbazole-5-ones: Optimization, mixed lineage kinase 1 crystallography and oral in vivo activity in 1-methyl-4-phenyltetrahydropyridine models. *J. Med. Chem.* **2008**, *51*, 5680−5689.

(15) van Erp, N. P.; Gelderblom, H.; Guchelaar, H. J. Clinical pharmacokinetics of tyrosine kinase inhibitors. *Cancer Treat. Rev.* **2009**, *35*, 692−706.

(16) (a) Fedorov, A. A.; Fedorov, E. V.; Pauletti, D.; Meyer, S. L.; Hudkins, R. L.; Almo, S. C. Crystal structure of cytoplasmic kinase domain of TIE-2 complexed with inhibitor CEP-11207. Protein Data Bank, 3L8P; 2010. (b) Traxler, P.; Furet, P. Strategies toward the design of novel and selective protein tyrosine kinase inhibitors. *Pharmacol. Ther.* **1999**, *82*, 195−206. (c) Backes, A. C.; Zeck, B.; Felber, B.; Klebl, B.; Müller, G. Small-molecule inhibitors binding to protein kinases. Part I: exceptions from the traditional pharmacophore approach of type I inhibition. *Expert Opin. Drug Discovery* **2008**, *3*, 1409−1425.

(17) (a) Vailhe, B.; Vittet, D.; Feige, J.-J. In vitro models of vasculogenesis and angiogenesis. *Lab. Invest.* **2001**, *81*, 439−452. (b) Ilan, N.; Mahooti, S.; Madri, J. A. Distinct signal transduction pathways are utilized during the tube formation and survival phases of *in vitro* angiogenesis. *J. Cell Sci.* **1998**, *111*, 3621−3631. (c) Brown, K.; J.; Maynes, S. F.; Bezos, A.; Maguire, D. J.; Ford, M. D.; Parish, C. R. A novel *in vitro* assay for human angiogenesis. *Lab. Invest.* **1996**, *75*, 539−555. (d) Nicosia, R. F.; Lin, Y. J.; Hazelton, D.; Qian, X. Endogenous regulation of angiogenesis in the rat aorta model. Role of vascular endothelial growth factor. *Am. J. Pathol.* **1997**, *151*, 1379−1386.